Supporting Information

Effect of Washing on Nickel-Rich NCMs: Methodology to Quantify the Lithium/Proton-Exchange Kinetics, the Inserted Protons, and the Structural Changes

Stefan Oswald, Rebecca Wilhelm, Tim Kratky, László Szentmiklósi, Boglárka Maróti, Ildikó Harsányi, Sebastian A. Hallweger, Gregor Kieslich, Sebastian Günther, and Hubert A. Gasteiger

Content

NCM particle morphology

The as-received and the three washed NCM831205 samples exhibit relatively large NCM primary crystallites of 0.2 to 2.0 µm in diameter, which are randomly agglomerated and sintered, and appear to form secondary agglomerates with a size of 2 to 6 µm. Due to the obvious particle agglomeration, the particle morphology of the NCM particles investigated in this study is characterized as a polycrystalline material, despite the relatively large primary crystallites and the non-spherical agglomerates as compared to typical polycrystalline particles.[1–3] The visual investigation of the NCM samples, comparing the as-received NCM and three washed samples in **Figure S1**, suggests that the particle morphology is largely unaffected by the washing.

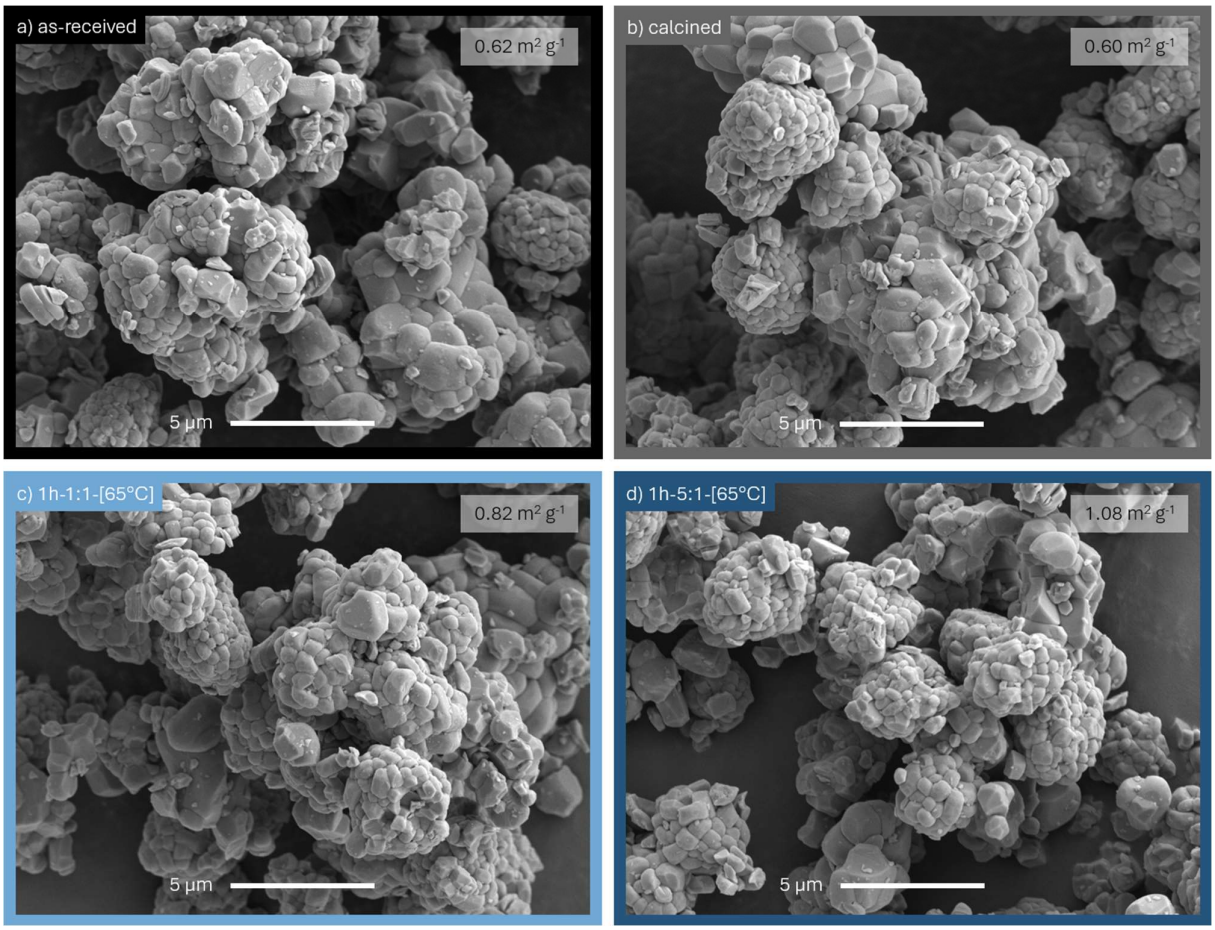

Figure S1. Visual investigation of the particle morphology of the a) as-received, b) calcined, as well as two washed NCM materials, i.e., of c) 1h-1:1-[65°C] and d) 1h-5:1-[65°C]. These representative top-view scanning electron microscopy images were collected in secondary-electron mode using an acceleration voltage of 5 kV.

However, based on the determined specific surface area A_{BET} (see **Table S1**), the washing results in a change of the specific surface area, which increases from 0.62 $m^2\ g^{-1}$ for the as-received sample to 1.67 $m^2\ g^{-1}$ for the sample with the harshest washing conditions with a proton content x_{H^+} of 25 mol%, as observed before by Strehle et al.[4] Using the spherical approximation in **Equation S1** and the crystallographic density ρ_{NCM} of the NCM material of 4.80 g cm^{-3},[5] approximate values between 0.7 and 2.1 µm are obtained for the particle diameter d_p (see **Table S1**).

$$d_{\mathrm{p}} = \frac{6}{\rho_{\mathrm{NCM}} \cdot A_{\mathrm{BET}}} \qquad \text{(S1)}$$

Since the images in **Figure S1** suggest that the apparent diameters of the primary and the secondary particles do not change upon washing, the change of the specific surface area implies that i) either washing exposes some of the interfaces between the primary particles, or ii) smaller primary crystallites are removed from the agglomerates. Thus, the removal of residual lithium salts and surface contaminants upon washing (see **Figure 1** of the main text) seems to give access to the pores between the primary crystallites of the secondary agglomerates.

Table S1. Overview of the values for the specific surface area A_{BET} obtained by Kr-BET as well as the respective calculated particle diameter for the as-received, the calcined, and differently washed NCM samples.

Sample	A_{BET} **(in m² g⁻¹)**	d_{p} **(in µm)**
as-received	0.62	2.0
calcined	0.60	2.1
2min-1:1-0°C-[120°C]	0.99	1.3
1h-1:1-[120°C]	0.82	1.5
1h-5:1-[120°C]	1.08	1.2
25h-5:1-[120°C]	1.27	0.9
55h-25:1-80°C-[120°C]	1.67	0.7

Estimation of the hydroxide content of the as-received NCM

In principle, the carbonate and hydroxide species can be differentiated and quantified by TGA-MS due to their differing decomposition temperatures of approx. 400 and 725 °C, respectively.[6] For an NCM, however, this approach is complicated by the possible presence of a protonated NCM phase, which might have formed upon lithium/proton exchange when stored in the presence of water vapor and would contribute to the mass loss during the TGA-MS experiment upon decomposition between 140 and 450 °C. Even though the decomposition temperature of the protonated NCM phase and the one of LiOH overlap, an upper limit of the LiOH content can be assessed. For this, the mass loss between 400 and 450 °C can be used to find the maximum LiOH amount which is present on the NCM. For the as-received NCM with a total mass loss of 0.09 wt% between 120 and 450 °C, a mass loss of approx. 0.01 wt% is observed by TGA-MS between 400 and 450 °C (see **Figure 3**). Since the decomposition of LiOH (with a molar mass of 24.0 g mol^{-1}) to Li_2O (29.9 g mol^{-1}) upon the release of H_2O (18.0 g mol^{-1}) is accompanied by a mass loss of 38 wt%, a maximum of 0.03 wt% of LiOH can be present on the as-received NCM, which converts to approx. 0.1 mol% of LiOH on the NCM (97.5 g/mol). For the obtained values of the proton content of 1 mol% or more, the contribution of 0.1 mol% of LiOH to the quantification of the proton content by titration would introduce a relative error of at most 10 %, which is (also considering the experimental error) acceptable. Since only the maximum amount of LiOH can be estimated by TGA-MS, the relative contribution of LiOH actually present on the as-received NCM might be much smaller.

TGA-MS data without sample

Figure 3 of the original manuscript presents the TGA-MS data of the as-received, calcined, and washed NCMs, which also display a decrease of the O_2 signal over the first 10 min during the initial hold at 25 °C (see **Figure 3d**) as well as an increase of both the H_2O and O_2 signal during the temperature ramps of 10 K min^{-1} (see **Figures 3c** and **3d**). To elucidate the origin of these features, we will discuss the data of a TGA-MS measurement with an empty crucible, i.e., without sample, as depicted in **Figure S2**.

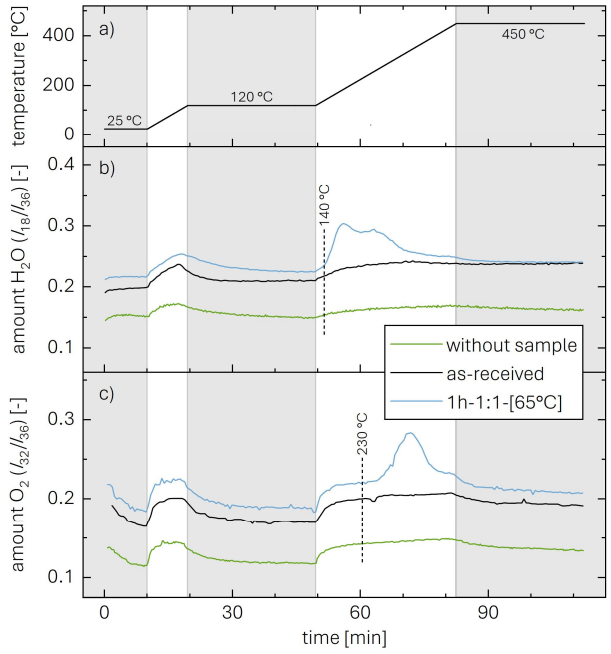

Figure S2. TGA-MS data of the as-received (black data) and the 1h-1:1-[65°C] washed (light blue) NCM sample taken from Figure 3 of the original manuscript, showing the **a)** the temperature profile, **b)** the amount of H_2O, and **c)** the amount of O_2. In addition, a measurement of an empty crucible, i.e., without sample, is investigated under the same experimental conditions (green).

During the first 10 min, the O_2 signal decreases for the initial temperature hold at 25 °C, independent of the presence of an as-received or washed NCM powder (see **Figure S2c**). Thus, this feature originates from the oxygen being present in the TGA furnace, after the furnace chamber was opened to load the crucible (with and without sample), allowing ambient gases to enter the furnace chamber. The initially present oxygen is constantly removed from the furnace chamber by the argon flow (of 60 ml min^{-1}), resulting in the initial decrease of the MS signal of O_2, which is not related to a (decomposition) reaction of the NCM sample.

Furthermore, during the temperature ramps of 10 K min^{-1} both from 25 to 120 °C and from 120 °C to 450 °C (white segments in **Figure S2**), an initial increase over the first few minutes and generally increased values as compared to the temperature holds are observed for both the H_2O and the O_2 signals. Furthermore, during the first few minutes of the temperature hold, i.e., after the temperature ramp has reached its final temperature of either 120 or 450 °C, a drop in both the H_2O and the O_2 signal can be observed (see **Figure S2b and S2c**). Again, these features are observed

independent of the presence of an as-received or washed NCM powder and are also present for the measurement without sample. Thus, we believe that these changes result from the increasing temperature in the furnace chamber, possibly inducing a desorption of water and oxygen from the furnace components as well as from cantilever and crucible. While the exact reason for this background rise is unclear, it can clearly be excluded that the here discussed features originate from the NCM sample.

In summary, it is concluded that the two features discussed here are induced by the background signal of the TGA-MS measurement and are not caused by a gas-desorption or thermal-decomposition reaction of the NCM sample. Thus, the H_2O release occurring beyond 140 °C and the O_2 release occurring beyond 230 °C for the washed samples show in fact the thermal decomposition of the washed NCM samples, as they are absent for both the measurement without sample as well as for the as-received and the calcined NCM samples.

TGA-MS data of 55h-25:1-80°C-[65°C]

Due to the much more pronounced mass loss and gas evolution during the TGA-MS experiment of the harshly washed NCM sample (55h-25:1-80°C-[65°C]) as compared to the other samples, the complete TGA-MS data are presented in **Figure S3** showing a mass loss of 4.42 wt% between 120 and 450 °C. The two-step decomposition reaction, which was also observed for 1h-1:1-[65°C] and 1h-5:1-[65°C] in **Figure 3**, shows the release of water at approx. 140 °C, while no oxygen is observed up to approx. 230 °C.

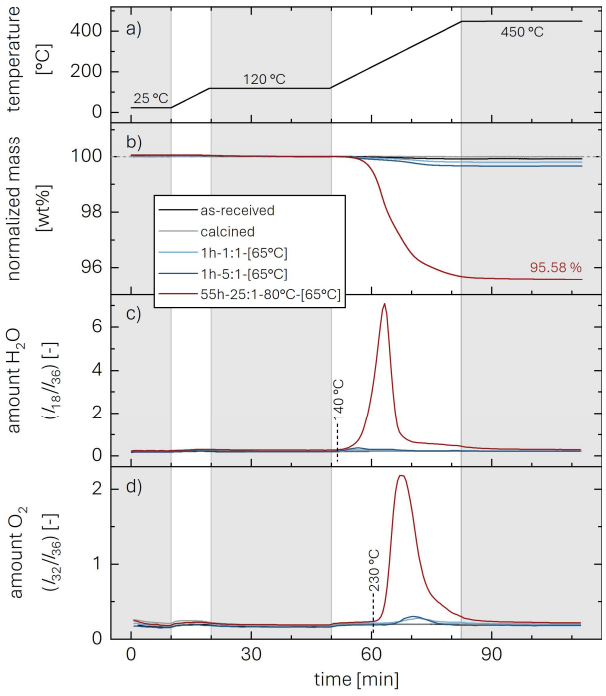

Figure S3. TGA-MS data of NCM powders as a function of time, presenting the data of Figure 3 using a scale chosen to completely depict the data of the harshly washed 55h-25:1-80°C-[65°C] sample.

Complete TR-XRD data for the as-received and the washed NCM

For the in-situ TR-XRD data of the as-received NCM as well as of the 55h-25:1-80°C-[65°C] sample (with x_{H^+} of 25.0 mol%), no additional peaks are observed during heating, whereby a slight increase in the diffraction background is observed only for 55h-25:1-80°C-[65°C]. The reflections agree well with the expected reflections of the layered (pale purple ticks at the bottom of **Figure S4**) and/or the rock-salt-type (black ticks) phase, while no additional reflections are observed in the regions where a spinel or corundum phase are expected (dark purple and purple ticks, respectively). The regions marked by the dashed black lines are magnified and presented in **Figure 4**.

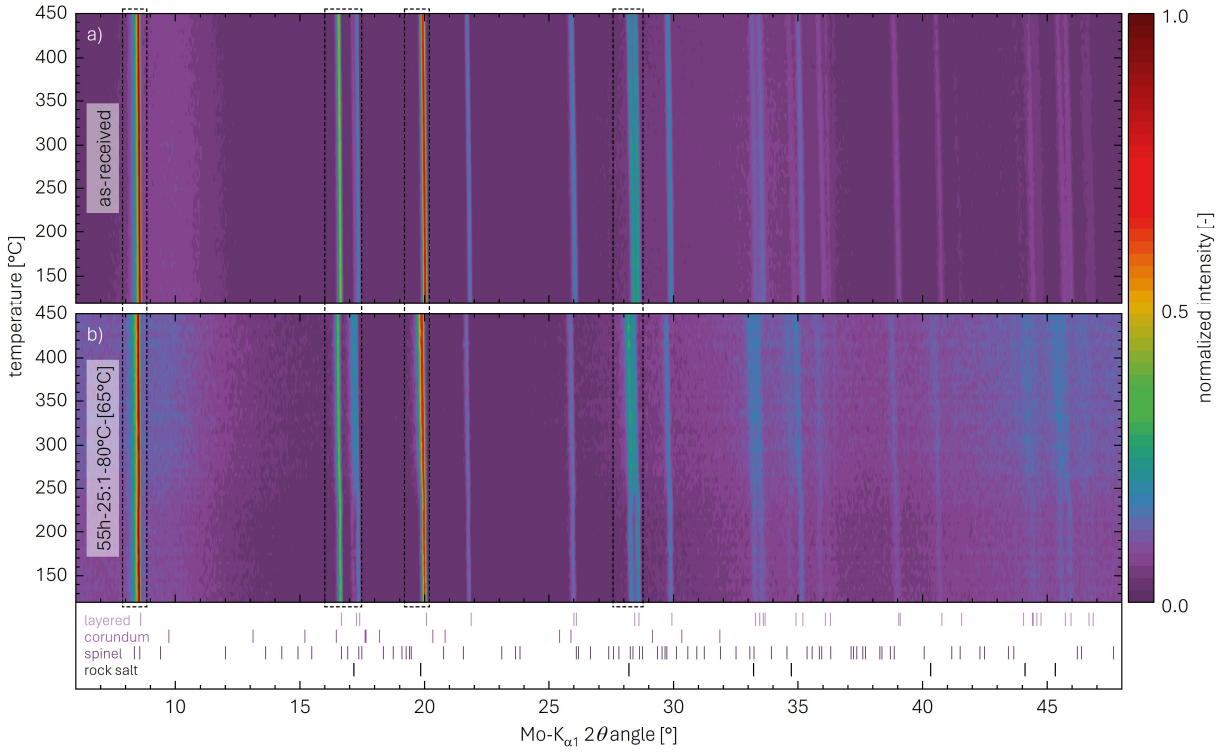

Figure S4. In-situ TR-XRD data of NCM samples acquired between 120 and 450 °C (at 5 K steps): **a)** as-received NCM; **b)** highly protonated 55h-25:1-80°C-[65°C] NCM (with x_{H^+} of 25.0 mol%). The diffractograms were acquired using Mo-$K_{\alpha1}$ radiation with a 2Θ angle between 6.0° and 48.0°. The vertical black dashed lines indicate the regions which are magnified in Figure 4.

Goodness of fit from ex-situ XRD

In addition to the difference plot in **Figure 5**, the error of the Rietveld refinement can also be expressed by the goodness-of-fit parameter χ, defined in the technical reference of the TOPAS 6 software,[7] which was used for the following quantitative analysis:

$$\chi = \sqrt{\frac{\sum_m w_m \cdot \left(Y_{o,m} - Y_{c,m}\right)^2}{M - P}} \qquad \text{(S2)}$$

Here, χ is based on the intensity $Y_{o,m}$ observed in the measurement for each data point m as well as the intensity $Y_{c,m}$ calculated by the fit, while the number of data points M of 2733, the number of parameters P of 13, and the weighting function w_m are considered.[7] Values of χ close to 1 are understood to provide a reliable fit, which is fulfilled for all the data presented in **Figure 5** and **Table 4**, with χ values between 0.86 and 1.15.

NCM lattice parameters from ex-situ XRD

The lattice parameters a_L and c_L of the layered NCM phase are obtained by a Rietveld refinement from the ex-situ XRD data shown in **Figure 5** for the as-received, the calcined, as well as the highly protonated and differently heated NCM sample (55h-25:1-80°C, with heat-treatment temperatures of 65, 120, 180, 230, 300, and 450 °C). The lattice parameters of the as-received and the calcined NCM exhibit the typical values of a_L of 2.87 and c_L of 14.19 Å (see **Figure S5**).[4,5] For the highly protonated NCM only heated to 65 °C, the lattice parameter c_L increases upon washing and heating to 65 °C, while a heat treatment above 230 °C induces a decrease to the value of the unwashed samples (see circles and solid lines in **Figure S5**); on the other hand, the lattice parameter a_L decreases, while it increases upon heat treatment at higher temperatures (triangles and dashed lines).

Similar changes of a_L, c_L, and c_L/a_L (see **Table 4**) are also observed when an NCM is delithiated electrochemically: upon delithiation, a_L decreases, c_L increases, and c_L/a_L increases.[5,8–10] Since c_L/a_L can be used as an indicator for the degree of delithiation, the change of c_L/a_L from 4.9433 to 4.9618 upon a protonation of approx. 25 mol% of the NCM (accompanied by an equimolar delithiation) would translate to a degree of electrochemically induced delithiation (i.e., in the absence of a Li^+/H^+ exchange) of approx. 10 mol%.[10] The smaller effect of the lithium/proton exchange (i.e., the exchange of ions) on the lattice parameters as compared to the one of a delithiation (i.e., the removal of ions) of the same amount is assigned to the difference of the steric and electrostatic properties of protons (i.e., of unshielded point charges) and lithium ions.

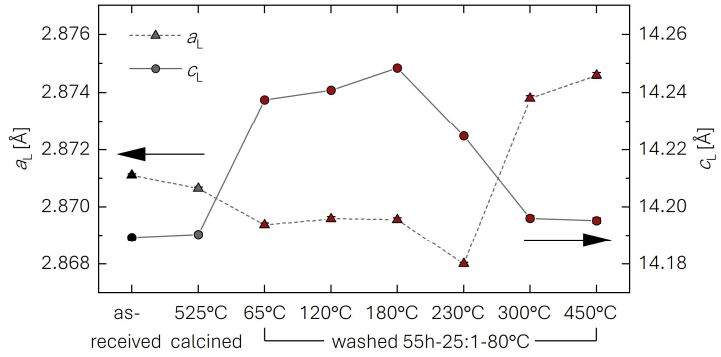

Figure S5. Lattice parameter a_L (triangles and dashed lines, left *y*-axis) and c_L (circles and solid lines, right *y*-axis) of the layered phase obtained by Rietveld refinement of ex-situ powder X-ray diffractograms for various NCM samples, extracted from the diffractograms presented in Figure 5: the as-received NCM (black), the calcined NCM (gray), as well as the washed and highly protonated 55h-25:1-80°C NCM sample (dark red) after heat-treatments at different temperatures (65, 120, 180, 230, 300, and 450 °C).

Calculation of the thickness of the near-surface rock-salt layer

The formula for the calculation of the thickness of the near-surface rock-salt layer, formed upon protonation and heat treatment, is derived in the following, assuming only core-shell particles as shown in **Figure S6**.

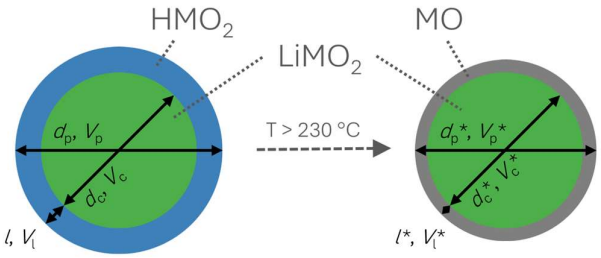

Figure S6. Schematic of a spherical NCM particle (labelled by p) with a lithiated core (labelled by c, green region), a protonated shell (blue) after washing (left particle) and a rock-salt shell (gray) after washing and heat treatment above 230 °C (right, labelled by *). The black arrows indicate the respective labels for the diameter *d* and the volume *V* of each region as well as the surface-layer thickness *l*.

For an average particle diameter d_p, extracted from the specific surface area via **Equation S1** (see **Table S1** for the actual values of the materials in this study), the volume of the whole particle is:

$$V_p = \frac{4}{3}\pi \cdot r_p^3 = \frac{4}{3}\pi \cdot \left(\frac{d_p}{2}\right)^3 \quad \text{(S3)}$$

For an identical cell volume per formula unit of the HMO_2 and $LiMO_2$ phase (note that their lattice parameters are essentially identical, see **Table 4**), the volume V_l of the protonated surface layer for a particle with a proton content of $x \equiv x_{H^+}$ (note that x is essentially identical to the molar fraction of the rock-salt phase after heat treatment, see **Equation 23**) equates to:

$$V_l = x \cdot V_p \quad \text{(S4)}$$

The volume V_c of the lithiated core is:

$$V_c = (1 - x) \cdot V_p \quad \text{(S5)}$$

Upon heat treatment above 180 °C and the release of H_2O and O_2 (see **Equation 21**), the layered protonated phase (HMO_2, containing one transition-metal atom) decomposes to a rock-salt phase (MO, also containing one transition-metal atom), having a cell volume per formula unit which is only 17.4 Å^3 based on the lattice parameters a_{RS} of the rock-salt phase of 4.11 Å (see main text), as compared to the layered phase ($LiMO_2$) of 33.8 Å^3, based on the lattice parameters of the calcined sample (presented in **Table 4**). Considering the parameters of the two phases results in a volume ratio β of MO and $LiMO_2$ phase of 0.51, the volume V_l^* of the decomposed surface layer for the heat-treated particle (indicated by *) is reduced to:

$$V_l^* = \beta \cdot V_l = \beta \cdot x \cdot V_p \quad \text{(S6)}$$

The volume V_c^* of the fully lithiated core of the particle does not change upon heat treatment, as the $LiMO_2$ phase is stable beyond 450 °C:

$$V_c^* = V_c = (1-x)\cdot V_p \quad \text{(S7)}$$

The volume V_p^* of the particle after heat treatment is the sum of the values for the volume of core and surface layer:

$$V_p^* = V_c^* + V_l^* = (1-x)\cdot V_p + \beta\cdot x\cdot V_p = \big(1 - x\cdot(1-\beta)\big)\cdot V_p \quad \text{(S8)}$$

The diameter d_p^* of the particle after heat treatment is given by:

$$d_p^* = 2\cdot\sqrt[3]{\frac{V_p^*}{\frac{4}{3}\pi}} = 2\cdot\sqrt[3]{\frac{(1-x\cdot(1-\beta))\cdot V_p}{\frac{4}{3}\pi}} = d_p\cdot\sqrt[3]{1-x\cdot(1-\beta)} \quad \text{(S9)}$$

The diameter d_c^* of the core of the particle after heat treatment, being identical to the diameter d_c of the core before heat treatment, is given by:

$$d_c^* = 2\cdot\sqrt[3]{\frac{V_c^*}{\frac{4}{3}\pi}} = 2\cdot\sqrt[3]{\frac{V_c}{\frac{4}{3}\pi}} = 2\cdot\sqrt[3]{\frac{(1-x)\cdot V_p}{\frac{4}{3}\pi}} = d_p\cdot\sqrt[3]{1-x} \quad \text{(S10)}$$

The thickness l^* of the near-surface rock-salt layer after heat-treatment relates to d_p^* and d_c^* by:

$$d_p^* = d_c^* + 2l^* \quad \text{(S11)}$$

Finally, l^* relates to x and β through:

$$l^* = \frac{1}{2}\big(d_p^* - d_c^*\big) = \frac{d_p}{2}\big(\sqrt[3]{1-x\cdot(1-\beta)} - \sqrt[3]{1-x}\big) \quad \text{(S12)}$$

For the given rock-salt content of 24 mol% of 55h-25:1-80°C-[450°C] after heat treatment (see **Figure 5**) with an estimated particle diameter d_p of 0.7 µm (see **Table S1**), the thickness l^* of the rock-salt surface layer amounts to 18 nm:

$$l^* = \frac{0.7\ \mu m}{2}\Big(\sqrt[3]{1-0.24\cdot(1-0.53)} - \sqrt[3]{1-0.24}\Big) = 18\ \text{nm} \quad \text{(S13)}$$

Furthermore, to obtain the thickness l of the protonated surface layer before heat treatment, **Equation S12** can be simplified, as the lattice parameters of the $LiMO_2$ and HMO_2 phase are essentially identical (see **Table 4**) and thus $\beta \approx 1$ for the protonated surface layer. This simplification results in the equation which was previously derived by Strehle et al.[11]:

$$l = \frac{d_p}{2}\big(1 - \sqrt[3]{1-x}\big) \quad \text{(S14)}$$

Thus, before heat treatment, the highly protonated sample 55h-25:1-80°C-[65°C] with a proton content of 24 mol% has a protonated surface layer with a thickness of 33 nm:

$$l = \frac{0.7\ \mu m}{2}\big(1 - \sqrt[3]{1-0.24}\big) = 33\ \text{nm} \quad \text{(S15)}$$

XPS survey spectra of the calcined and differently washed NCM samples

The XPS data obtained by a survey scan between 1202.5 and 0 eV is presented in **Figure S7,** assigning the relevant core-level photoelectron and Auger emissions that can be discerned in the survey scan. Note that the Ni 3p, the Co 3p, the Li 1s, and the Mn 3p signals are located in the region marked by the orange dashed lines; these are not labeled since, in the survey scan, they cannot be clearly distinguished from each other, which is why a high-resolution core-level scan is in the focus of **Figure 6**. The C 1s signals at 284.5 eV are observed at a similar intensity for every sample, originating from adventitious carbon, which is typical for sample surfaces that have not been pre-treated in ultra-high vacuum prior to XPS analysis (e.g., by ion-beam sputtering). For the calcined NCM (gray line in **Figure S7**), additional peaks due to sodium (Na 1s) and sulfur (S 2p) can be discerned, which are indicative of sodium sulfate (Na_2SO_4);[12] the latter is a typical residue from the NCM synthesis (the mixed-TM-hydroxide precursor is typically precipitated from TM sulfates and sodium hydroxide/carbonate);[13,14] upon heating, Na_2SO_4 is reported to migrate to the particle surface,[15] explaining the absence of both signals for the as-received sample (data not shown) and for the washed samples that had only been heat-treated at 65 °C.

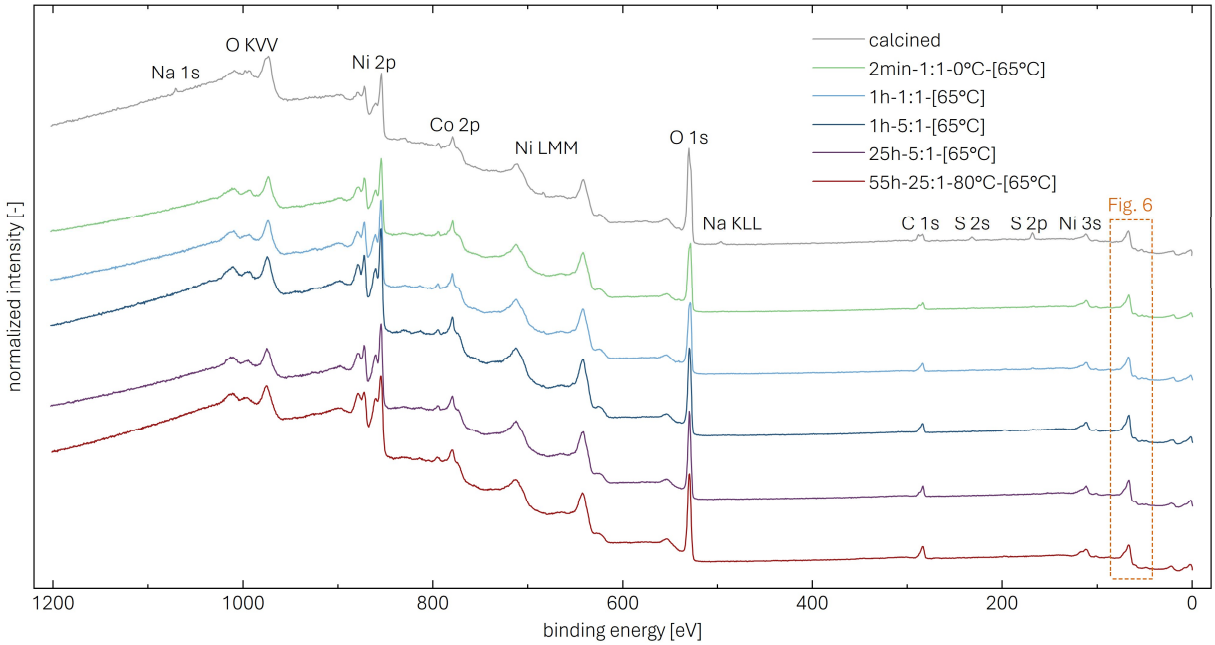

Figure S7. XPS data of the calcined and of differently washed NCM samples that were heat-treated at 65 °C. Shown is a survey scan with a step size of 0.5 eV, a dwell time of 100 ms, and a pass energy of 160 eV, recorded using monochromatized Al-K_α radiation with an energy of 1486.6 eV. The data are normalized by the total integrated Ni 3p (at approx. 70 eV binding energy) intensity and corrected for sample charging by using the C 1s signal of adventitious carbon at 284.5 eV. The core levels and Auger transitions are assigned. The orange dashed lines indicate the region which is examined in more detail in Figure 6.

Estimation of the proton content by XPS

Due to the surface sensitivity of XPS, only the near-surface region is probed, so that the amount of bulk lithium in the NCM particles cannot be determined. However, to allow for a comparison of the XPS data with those of the bulk-sensitive techniques (see **Table 6**), the proton content x_{H^+} can be estimated by approximating the NCM material as monodisperse spheres with a single particle diameter. For each of the samples investigated by XPS, the particle diameter is calculated based on the determined specific surface area A_{BET}, as displayed in **Table S1**. The proton content can be described by the volume V_l of the protonated surface layer with respect to the total volume V_p of a spherical particle:

$$x_{H^+} = \frac{V_l}{V_p} = \frac{V_p - V_c}{V_p} = \frac{d_p^3 - d_c^3}{d_p^3} = \frac{d_p^3 - (d_p - 2l)^3}{d_p^3} = \frac{d_p^3 - (d_p - 2l)^3}{d_p^3} \quad \text{(S16)}$$

The calculated x_{H^+} values, depicted in **Table S2**, do not agree exactly with the ones measured by the other techniques (see **Table 6**) and are smaller by roughly a factor of 2.

Table S2. Overview of the XPS-derived thickness l of the delithiated surface layer (same as Table 5) as well as the proton content x_{H^+} (based on Equation S14), using the values for the particle diameter d_p listed in Table S1. For the calcined sample, it is assumed that no protons are present, indicated by 0* and 0** for l and x_{H^+}, respectively. The values for l and x_{H^+} of 55h-25:1-80°C-[65°C] are below the detection limit, indicated by >8.1 and >6.4, respectively.

Sample	l **(in nm)**	x_{H^+} **(in mol%)**
calcined	0*	0**
2min-1:1-0°C-[65°C]	0.4	0.2
1h-1:1-[65°C]	0.7	0.3
1h-5:1-[65°C]	1.5	0.8
25h-5:1-[65°C]	2.6	1.6
55h-25:1-80°C-[65°C]	>8.1	>6.4

This discrepancy is ascribed to the particle size distribution of the NCM material, which is clearly very broad and certainly not monodisperse, as observed in the SEM images of the NCM samples (see **Figure S1**). Thus, using the XPS-derived thickness l of the protonated near-surface region is not a sensible approach to quantify x_{H^+} of washed NCMs. However, the XPS-derived l value for the thickness of the protonated surface layer is reliable, independent of the particle size distribution, and is proportional to the proton content x_{H^+} obtained by the other techniques (see **Figure 7**), confirming the hypothesis of particles with a purely lithiated core and purely protonated shell.

Comparison of the (dis)advantages of the employed methods

The most relevant aspects of the five different methods have been summarized in **Table S3** to provide guidelines for choosing the most suitable approach to quantify the proton content in NCMs.

Table S3. Comparison of the five different methods used to quantify the proton content of the NCM material, including effort regarding experiment and analysis, accessibility, accuracy, required sample amount, as well as advantages and disadvantages/limitations of each method.

	Titration	**PGAA**	**TGA(-MS)**	**XRD**	**XPS**
Effort (experiment)	low	high	low	medium	medium
Effort (analysis)	low	high (fitting of spectra)	low	medium (Rietveld refinement)	high (fitting of spectra)
Accessibility	widely accessible	proposal for/access to nuclear reactor required	widely accessible	widely accessible	accessible
Accuracy/ Sensitivity	high	medium	very high	medium	high (thickness of surface-layer only)
Required sample amount	medium (≈100 mg_{CAM})	medium (≈100 mg_{CAM})	medium (≈100 mg_{CAM})	very low (≈1 mg_{CAM})	low (≈10 mg_{CAM})
Advantages	high sensitivity, direct quantification of Li_2CO_3	provides overall stoichiometry including transition metals	additionally provides decomposition mechanism and amount of surface contaminants	additionally provides information on decomposition mechanism	surface-specific; quantification of layer thickness
Disadvantages/ limitations	sensitive to ambient atmosphere due to conversion of LiOH to Li_2CO_3 by dissolution of CO_2	lower limit for proton content of approx. 1 mol%; extensive data analysis required	fully inert transfer challenging	lower limit for proton content of approx. 1 to 10 mol% (depending on the brilliance of the X-ray source); extensive data analysis required	no bulk information, only semi-quantitative regarding proton content; low sensitivity to lithium; upper limit for proton content

References

1 L. Cheng, B. Zhang, S. L. Su, L. Ming, Y. Zhao, C. H. Wang and X. Ou, *J. Alloys Compd.*, 2020, **845**, 156202.

2 S. Oswald, D. Pritzl, M. Wetjen and H. A. Gasteiger, *J. Electrochem. Soc.*, 2021, **168**, 120501.

3 S. Oswald, M. Bock and H. A. Gasteiger, *J. Electrochem. Soc.*, 2023, **170**, 090505.

4 B. Strehle, F. Friedrich and H. A. Gasteiger, *J. Electrochem. Soc.*, 2021, **168**, 050512.

5 L. de Biasi, A. O. Kondrakov, H. Geßwein, T. Brezesinski, P. Hartmann and J. Janek, *J. Phys. Chem. C*, 2017, **121**, 26163–26171.

6 J. Sicklinger, M. Metzger, H. Beyer, D. Pritzl and H. A. Gasteiger, *J. Electrochem. Soc.*, 2019, **166**, A2322–A2335.

7 A. Coelho, TOPAS-Academic V6, Coelho Software, Brisbane, Australia, 2015.

8 J. Choi and A. Manthiram, *J. Electrochem. Soc.*, 2005, **152**, A1714–A1718.

9 A. O. Kondrakov, A. Schmidt, J. Xu, H. Geßwein, R. Mönig, P. Hartmann, H. Sommer, T. Brezesinski and J. Janek, *J. Phys. Chem. C*, 2017, **121**, 3286–3294.

10 F. Friedrich, B. Strehle, A. T. S. Freiberg, K. Kleiner, S. J. Day, C. Erk, M. Piana and H. A. Gasteiger, *J. Electrochem. Soc.*, 2019, **166**, A3760–A3774.

11 B. Strehle, K. Kleiner, R. Jung, F. Chesneau, M. Mendez, H. A. Gasteiger and M. Piana, *J. Electrochem. Soc.*, 2017, **164**, A400–A406.

12 N. H. Turner, J. S. Murday and D. E. Ramaker, *Anal. Chem.*, 1980, **52**, 84–92.

13 R. Schmuch, R. Wagner, G. Hörpel, T. Placke and M. Winter, *Nat. Energy*, 2018, **3**, 267–278.

14 R. B. Berk, T. Beierling, L. Metzger and H. A. Gasteiger, *J. Electrochem. Soc.*, 2023, **170**, 110513.

15 L. Hartmann, D. Pritzl, H. Beyer and H. A. Gasteiger, *J. Electrochem. Soc.*, 2021, **168**, 070507.